

# Non-neutral plasma equilibria with weak axisymmetric magnetic perturbations

I. A. Kotelnikov

*Budker Institute of Nuclear Physics, Lavrentyev Avenue 11, Novosibirsk, 630090, Russia*

M. Romé<sup>a)</sup>

*I.N.F.N. Sezione di Milano and Dipartimento di Fisica, Università degli Studi di Milano, Via Celoria 16, I-20133, Milano, Italy*

A. Kabantsev

*Physics Department, University of California at San Diego, 9500 Gilman Drive, La Jolla, California 92093-0319*

(Received 14 June 2006; accepted 31 July 2006; published online 12 September 2006)

The effect of weak axisymmetric magnetic and/or electrostatic perturbations on the equilibrium of a non-neutral plasma in a Malmberg-Penning trap is analyzed. Analytical and semianalytical solutions for the potential variations inside the trap are found in a paraxial limit of the perturbations for various radial density profiles of the plasma, including the case of global thermal equilibrium. It is shown that a magnetic perturbation produces a potential variation with a sign which is changing along the plasma radius. The fraction of magnetically and electrostatically trapped particles thus created is calculated explicitly for the case of a Maxwellian distribution function, and it is shown to be independent from the sign of the magnetic field perturbation. The analysis of the potential perturbation is extended to the case of an anisotropic distribution function, with an arbitrary ratio between the parallel and the perpendicular plasma temperature. Two-dimensional thermal equilibrium simulations for parameters relevant to the CamV device [A. A. Kabantsev, J. H. Yu, R. B. Lynch, and C. F. Driscoll, *Phys. Plasmas* **10**, 1628 (2003)] confirm the predictions of the analytical theory for smooth and weak perturbations of the magnetic field. © 2006 American Institute of Physics. [DOI: [10.1063/1.2344930](https://doi.org/10.1063/1.2344930)]

## I. INTRODUCTION

The radial confinement of non-neutral plasmas in Malmberg-Penning traps is provided by a strong axial magnetic field. This field is assumed to be uniform in most theories that deal with plasma confinement. However it has long been suspected that small perturbations of the magnetic field may play a crucial role in the transport of non-neutral plasmas in this kind of confinement devices;<sup>1</sup> see also the review papers (Refs. 2 and 3), and references therein for further discussion of the problem of plasma transport in Malmberg-Penning traps. On the other hand, it is well known that an accurate treatment of the plasma transport requires at first an analysis of the plasma equilibrium, as it is proven by established theories of transport for quasineutral plasma confined, e.g., in tandem mirrors.<sup>4</sup> This fact was neglected in some previous theories of non-neutral plasma transport induced by magnetic field errors (see, e.g., Ref. 5). In this paper the effect of magnetic field perturbations on the equilibrium of a non-neutral plasma is considered. The study is limited to the case of axisymmetric perturbations. Although such perturbations alone do not enhance plasma transport, their investigation helps to elucidate some fundamental features of non-neutral plasma equilibria that makes impossible a straightforward extension of the theory of resonant or neoclassical transport developed for quasineutral plasma in tan-

dem mirrors to the case of non-neutral plasma in Malmberg-Penning traps.

The effects of perturbations in the axial magnetic fields have recently been investigated for another reason: mirror fields come into play when trapped non-neutral plasmas are transported from one trap to another, as it is common in antimatter traps. Moreover, researchers have speculated that undesired mirror fields are responsible for transport in Malmberg-Penning traps.<sup>6,7</sup>

The equilibrium properties of non-neutral plasmas in uniform magnetic fields were identified long ago.<sup>8,9</sup> Dubin and O'Neil developed a general framework that includes global thermal equilibrium states in mirror fields, but did not analyze these states closely.<sup>3</sup> Fajans pointed out some peculiar features of non-neutral plasma equilibria in Malmberg-Penning traps with mirror magnetic fields;<sup>10</sup> some of his conclusions are mentioned later, and critically discussed when appropriate.

The approach adopted here is based on the use of curvilinear flux coordinates for the magnetic field. If a magnetic perturbation is turned on "adiabatically" in a given section of the confinement device, then the associated perturbation of the electric potential in a given point turns out to be generally (much) greater than the potential perturbation on a fixed magnetic field line. In other words, a magnetic flux surface within the charged plasma column remains *quasi*-equipotential if the magnetic field becomes nonuniform. This makes the use of curvilinear coordinates preferable when

<sup>a)</sup>Electronic mail: [rome@mi.infn.it](mailto:rome@mi.infn.it)

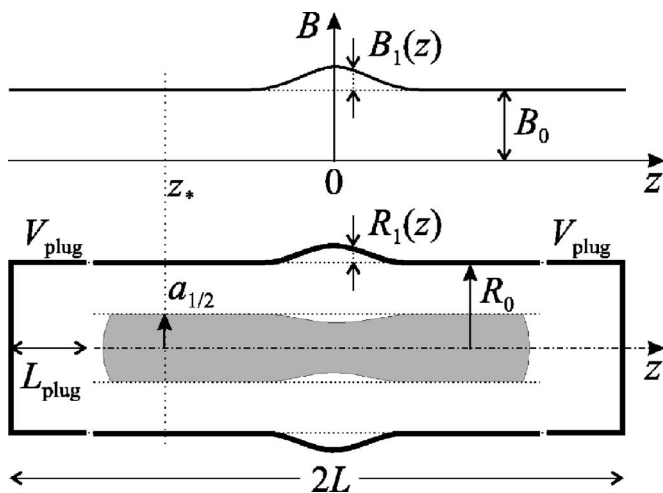


FIG. 1. Geometry of the model. Effect of an axisymmetric perturbation of the magnetic field on the equilibrium of a long non-neutral plasma column.

computing the electric field in charged plasmas confined in slightly nonuniform magnetic fields.

The paper is organized as follows: In Sec. II, the main features of the model used to analyze the effect of magnetic field perturbations are outlined. In Sec. III the equilibrium of a non-neutral plasma is computed in a paraxial limit for weak axial perturbations of magnetic and electric fields; different radial density profiles are considered, including the case of global thermal equilibrium. In particular, the main differences between the perturbations of the electric potential induced by variations of the magnetic field or by variations of the conducting wall radius are pointed out. The analysis is extended to the case of an anisotropic plasma, and the fraction of magnetically and electrostatically trapped particles is computed for a Maxwellian and a bi-Maxwellian distribution function. Several phenomena that lead to deviations from paraxial equilibrium are discussed in Sec. IV. In Sec. V, the results of the one-dimensional analytical theory are checked against two-dimensional simulations of the thermal equilibrium of a pure electron plasma in the presence of axial magnetic field perturbations, for parameters relevant to the CamV experiment<sup>11</sup> at the University of California, San Diego (UCSD). The main results of the paper are summarized and discussed in Sec. VI.

## II. MODEL

A model of a long pure electron plasma column contained in a cylindrical conducting chamber of radius  $R$  and immersed in an axisymmetric magnetic field  $B$  is adopted, with  $z$  being the coordinate along the symmetry axis, as shown in Fig. 1. Column-end effects are neglected and the attention is focused on the central part of the confining chamber, with a grounded conducting wall,  $\varphi_W=0$ . In the unperturbed state, characterized by a uniform magnetic field  $B_0$  and a constant wall radius  $R_0$ , the plasma density is constant along field lines. The goal is to fully characterize the electric potential in the plasma in those regions of the device

where the magnetic field  $B=B_0+B_1(z)$  and the wall radius  $R=R_0+R_1(z)$  are perturbed by small quantities  $B_1(z)\ll B_0$  and  $R_1(z)\ll R_0$ , respectively.

To describe the equilibrium potential in a nonuniform magnetic field it is useful to introduce curvilinear flux coordinates  $(\alpha, \beta, \chi)$  such that

$$\mathbf{B} = \nabla\alpha \times \nabla\beta = \nabla\chi. \quad (1)$$

The functions  $\alpha$  and  $\beta$  are constant along magnetic field lines, and  $\chi$  is the magnetic potential. For an axisymmetric field, it is possible to identify  $\beta$  as the azimuthal angle,  $\beta=\theta$ , and  $\alpha$  is therefore the magnetic flux,  $\alpha=rA_\theta(r, z)$ . Poisson's equation is written in flux coordinates as

$$\frac{\partial}{\partial\alpha} r^2 \frac{\partial\varphi}{\partial\alpha} + \frac{1}{r^2 B^2} \frac{\partial^2\varphi}{\partial\beta^2} + \frac{\partial^2\varphi}{\partial\chi^2} = -\frac{4\pi en}{B^2}. \quad (2)$$

Note that throughout the paper  $e$  denotes the charge of the particles, so that  $e<0$  for electrons. The particles are assumed to be in thermal equilibrium along individual field lines, though not necessarily in global thermal equilibrium. This means that the electron distribution function  $f$  is constant along magnetic field lines, i.e., it does not depend on  $\chi$ . For an axisymmetric equilibrium, the distribution function does not depend on  $\beta$  as well, and hence in drift approximation it can be written as a function of electron energy,  $\varepsilon$ , magnetic moment,  $\mu$ , and magnetic flux,  $\alpha$ , i.e.,  $f=f(\varepsilon, \mu, \alpha)$ . The plasma density in the RHS of Poisson's equation (2) is evaluated as

$$n = \frac{4\pi B}{m^2} \int_0^\infty d\mu \int_{\mu B + e\varphi}^\infty \frac{d\varepsilon}{v_\parallel} f. \quad (3)$$

For a Maxwellian distribution function,

$$f(\varepsilon, \alpha) = (m/2\pi T)^{3/2} N(\alpha) \exp(-\varepsilon/T), \quad (4)$$

the density (3) obeys Boltzmann law

$$n = N(\alpha) \exp(-e\varphi/T). \quad (5)$$

In Sec. IV C, the physical backgrounds justifying the use of Boltzmann law (5) will be critically revisited.

The equilibrium assumes a particularly simple form for flat-top plasmas, and this case is analyzed first in Sec. III A. In Sec. III B, the analysis is extended to the radial profile that characterizes a global thermal equilibrium state.<sup>8,12</sup> In Sec. V results of a one-dimensional (1D) semianalytical theory based on a reduced Poisson's equation are tested against two-dimensional (2D) plasma equilibrium computations in the presence of axial magnetic field perturbations.

## III. "PARAXIAL" APPROXIMATION

In a long-thin (paraxial) approximation, i.e., when the variations of  $B$  and  $R$  are both: (i) axisymmetric; and (ii) smooth, so that their characteristic axial length,  $\ell$ , substantially exceeds the wall radius,  $\ell \gg R$ , Poisson's equation (2) can be further reduced to

$$\frac{\partial}{\partial \alpha} \alpha \frac{\partial \phi}{\partial \alpha} = -\frac{2\pi en}{B}. \quad (6)$$

The axial symmetry cancels the derivatives over the azimuthal angle  $\beta$ , while the paraxial assumption justifies neglecting the derivatives along field lines in the Poisson's equation. The transformation to curvilinear coordinates becomes also easier since the functions  $\alpha$  and  $\chi$  can be expressed by means of the magnetic field on the axis:

$$\alpha \approx [B_0 + B_1(z)]r^2/2, \quad (7a)$$

$$\beta = \theta, \quad (7b)$$

$$\chi \approx \int^z [B_0 + B_1(z)]dz. \quad (7c)$$

The following computations become more transparent if the flux radius

$$\rho = \sqrt{2\alpha/B_0} \quad (8)$$

is introduced instead of the magnetic flux  $\alpha$ ;  $\rho$  labels a magnetic field line starting at a radius  $r$  outside of the perturbation region,

$$\rho \approx r[1 + B_1/2B_0]. \quad (9)$$

The coordinate  $\rho$  will be used interchangeably with  $\alpha$  in the following, assuming implicitly that, e.g.,  $N(\rho)$  means  $N(\alpha)$  with  $\alpha$  expressed in terms of  $\rho$ .

Making use of Eqs. (5) and (8), Poisson's equation (6) can be cast into the form

$$\frac{1}{\rho} \frac{\partial}{\partial \rho} \rho \frac{\partial \phi}{\partial \rho} = -\frac{4\pi e^2 N(\rho) B_0}{T} \exp(-\phi), \quad (10)$$

where  $\phi = e\varphi/T$  is the dimensionless potential. Interpreting the nonuniform part of the magnetic field as a small perturbation, a standard perturbation procedure is applied to Eq. (10). The unperturbed potential  $\phi_0(\rho)$  obeys the equation

$$\frac{1}{\rho} \frac{\partial}{\partial \rho} \rho \frac{\partial \phi_0}{\partial \rho} = -\frac{N_0(\rho)}{\lambda_D^2}, \quad (11a)$$

where  $N_0(\rho) = N(\rho) \exp[-\phi_0(\rho)]/n_*$  is the unperturbed density, normalized to its value  $n_* = N(0) \exp(-\phi_0(0))$  on the axis, and  $\lambda_D = \sqrt{T/4\pi e^2 n_*}$  is the Debye length. The unperturbed potential  $\phi_0$  is subject to the boundary condition

$$\phi_0(R_0) = 0. \quad (11b)$$

Since the unperturbed density  $N_0(\rho)$  is a given function in the present treatment, one readily obtains that

$$\phi_0(\rho) = \frac{1}{\lambda_D^2} \int_{\rho}^{R_0} \frac{d\rho''}{\rho''} \int_0^{\rho''} d\rho' \rho' N_0(\rho').$$

The perturbed potential  $\phi_1$  obeys the equation

$$\frac{1}{\rho} \frac{\partial}{\partial \rho} \rho \frac{\partial \phi_1}{\partial \rho} = \frac{N_0(\rho)}{\lambda_D^2} (\phi_1 + \delta B), \quad (12a)$$

supplemented with the boundary condition

$$\phi_1(R_0) = -R_0 \phi_0'(R_0) (\delta R + \delta B/2), \quad (12b)$$

which represents the linearized form of the boundary condition  $\phi_0 + \phi_1 = 0$  for the total potential at the perturbed flux radius of the wall,  $\rho_w = R_0(1 + \delta R + \delta B/2)$ , with  $\delta R \equiv R_1/R_0$  and  $\delta B \equiv B_1/B_0$ .

Using  $\rho$  instead of the cylindrical radius  $r$  simplifies solving Poisson's equation due to the fact that the density of an isotropic plasma, Eq. (5), depends merely upon the flux radius  $\rho$  and the electric potential  $\phi$ , no matter the magnetic field is uniform or not. It is shown here in the following that the perturbation of the electric potential in ordinary cylindrical coordinates is, in a certain sense, much greater than that expressed in flux coordinates, but the dominant term of this perturbation does not affect the particle motion along a magnetic field line.

### A. Stepwise density profile

A simple analytical solution exists for a stepwise density profile

$$N_0(\rho) = H(a_0 - \rho),$$

where  $H$  is the Heaviside's step function, and  $a_0$  is the unperturbed radius of the plasma column. In this case, the solution of Eqs. (11a) and (11b) takes the form

$$\phi_0(\rho) = -\frac{\rho^2 - a_0^2 + 2a_0^2 \ln(a_0/R_0)}{4\lambda_D^2} \quad (13a)$$

for  $\rho \leq a_0$ , and

$$\phi_0(\rho) = -\frac{a_0^2}{2\lambda_D^2} \ln \frac{\rho}{R_0} \quad (13b)$$

for  $\rho > a_0$ . Correspondingly, Eqs. (12a) and (12b) yield a perturbed potential

$$\phi_1(\rho, z) = \frac{\left(1 + \frac{a_0^2}{4\lambda_D^2}\right) \delta B + \left(\frac{a_0^2}{2\lambda_D^2}\right) \delta R}{I_0\left(\frac{a_0}{\lambda_D}\right) + \frac{a_0}{\lambda_D} I_1\left(\frac{a_0}{\lambda_D}\right) \ln \frac{R_0}{a_0}} I_0\left(\frac{\rho}{\lambda_D}\right) - \delta B \quad (14a)$$

inside the plasma, and

$$\begin{aligned} \phi_1(\rho, z) = & \frac{\left(1 + \frac{a_0^2}{4\lambda_D^2}\right) \delta B + \left(\frac{a_0^2}{2\lambda_D^2}\right) \delta R}{I_0\left(\frac{a_0}{\lambda_D}\right) + \frac{a_0}{\lambda_D} I_1\left(\frac{a_0}{\lambda_D}\right) \ln \frac{R_0}{a_0}} \frac{a_0}{\lambda_D} I_1\left(\frac{a_0}{\lambda_D}\right) \ln \frac{\rho}{R_0} \\ & + \frac{a_0^2}{4\lambda_D^2} (\delta B + 2\delta R) \end{aligned} \quad (14b)$$

outside of the plasma. This solution has been earlier discussed by Fajans for the particular case  $R_1=0$ ; cf. Eqs. (2) and (3) in Ref. 10 with Eq. (14a).

The function  $\phi_1(\rho, z)$  characterizes the variation of the electric potential (normalized over  $T/e$ ) along a magnetic field line with a given flux radius  $\rho$ , and therefore describes the trapping of particles with small longitudinal velocity. When moving along a magnetic field line, a particle undergoes a smoothly varying magnetic field perturbation and a

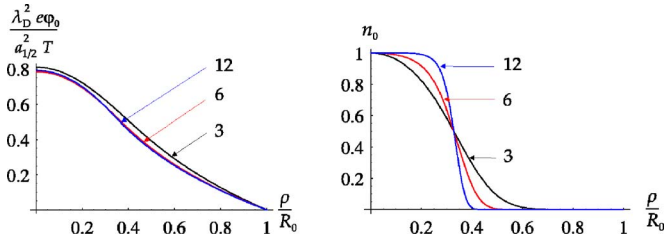


FIG. 2. (Color online) Thermal equilibrium potential  $\varphi_0$  (left) and plasma density  $n_0$  (right) for a fixed plasma radius  $a_{1/2}=1.151$  cm [evaluated at the level of 1/2 of the maximum density  $n_0(0)$  at the plasma axis], and three different ratios  $a_{1/2}/\lambda_D=\{3,6,12\}$  (indicated by the arrows), corresponding to  $\gamma=\{1.893\times 10^{-1}, 1.176\times 10^{-2}, 4.140\times 10^{-5}\}$  and  $e\varphi_0(0)/T=\{7.294, 28.24, 114.0\}$ , respectively. The case  $a_{1/2}/\lambda_D=6$  approximately corresponds to the CamV experiment, characterized by  $n_s=1.5\times 10^7$  cm $^{-3}$ ,  $T=1$  eV,  $\lambda_D=0.19$  cm,  $R_0=3.5$  cm.

corresponding change in the electric potential  $\phi_1(\rho, z)$ , where  $\rho$  is fixed while  $z$  enters parametrically through the perturbed profiles of magnetic field,  $\delta B(z)$ , and wall radius,  $\delta R(z)$ . The perturbation of the plasma density along the field line follows the profile of the electric potential since  $n_1(\rho, z)=-n_0(\rho)\phi_1(\rho, z)$ , where  $n_0(\rho)=n_*N_0(\rho)$ .

When perturbed quantities are computed in ordinary coordinates, one needs to take into account the displacement of magnetic field lines in the perturbation region. In particular, the electric potential is characterized by the function

$$\phi(r, z) = \phi_0(r(1 + \delta B/2)) + \phi_1(r(1 + \delta B/2), z).$$

Retaining all terms, which are linear in  $\delta B$  and  $\delta R$ , one finds the perturbation

$$\phi_1^*(r, z) = \phi_0'(r)r\delta B/2 + \phi_1(r, z) \quad (15)$$

that describes the variation of the electric potential along a straight line at a given radius  $r$ . The first term in the right-hand side (RHS) of Eq. (15) is approximately  $(a_0/\lambda_D)^2$  times larger than the second term, i.e.,  $\phi_1^* \gg \phi_1$ , but the former does not affect the particle motion along a magnetic field line. Similarly, for the perturbation of the plasma density it results in

$$n_1^*(r, z) = n_0'(r)r\delta B/2 + n_1(r, z). \quad (16)$$

Analogously to  $\phi_1^*$ , the function  $n_1^*(r, z)$  describes the perturbed density profile along a straight line at a given distance  $r$  from the column's axis, however in this case both terms in the RHS of Eq. (16) have the same order of magnitude.

It is worth noting that variations of plasma density and potential can be caused by a variation of the potential on the chamber wall as well. However this does not require a separate treatment since the potential variation along the chamber wall  $\phi_1(R_0)$  is completely modeled by the variation of the wall radius  $R_1$ : the two quantities are related by the equation  $\phi_1(R_0)=-\phi_0'(R_0)R_1$ , where the prime stands for the radial derivative.

A straightforward analysis of Eq. (14a) reveals that the potential perturbation induced by the magnetic field ripples qualitatively differs from that induced by chamber wall ripples. The former may have in fact opposite signs in the

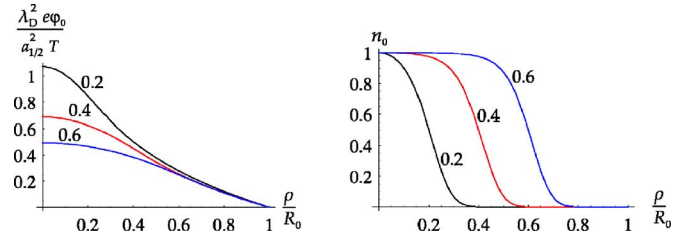


FIG. 3. (Color online) Thermal equilibrium potential  $\varphi_0$  (left) and plasma density  $n_0$  (right) for different plasma radii  $a_{1/2}=\{0.2, 0.4, 0.6\}\times R_0$ , corresponding to  $\gamma=\{1.015\times 10^{-1}, 3.547\times 10^{-3}, 1.134\times 10^{-4}\}$  and  $e\varphi_0(0)/T=\{14.25, 36.61, 59.12\}$ , respectively. The parameters  $\lambda_D$  and  $R_0$  are the same as in Fig. 2.

inner and outer parts of the plasma column, while the latter has always the same sign at all radii. If  $\lambda_D \ll \rho \leq a_0$  and  $\delta R=0$ , Eq. (14a) reduces to

$$\phi_1 = \left[ \frac{(1 + a_0^2/4\lambda_D^2)e^{(\rho-a_0)/\lambda_D}}{1 + (a_0/\lambda_D)\ln(R_0/a_0)} - 1 \right] \delta B.$$

The potential perturbation is negative (if  $\delta B > 0$ ) on the column's axis, where  $\phi_1 = -\delta B$ , but monotonically increases to the column periphery, and may become positive if

$$a_0/\lambda_D > 4 \ln(R_0/a_0), \quad (17)$$

otherwise the sign reversal occurs outside of the plasma. If inequality (17) holds,  $\phi_1$  goes through zero within a thin boundary layer with a width of the order of  $\lambda_D$ . Under usual experimental conditions, the column boundary can hardly be sharper than few Debye lengths. One can therefore expect that an outer part of the plasma column always exists, where the perturbed potential has a sign opposite to that on the plasma axis. In the next section, this issue will be analyzed for the density profile corresponding to the state of global thermal equilibrium.

## B. Thermal equilibrium density profile

In the state of global thermal equilibrium the unperturbed density profile has the form<sup>8,12</sup>

$$N_0(\rho) = \exp(\psi_* - \psi),$$

where the effective potential

$$\psi(\rho) = \frac{e\varphi}{T} + \frac{\rho^2}{4\lambda_D^2}(1 + \gamma) \quad (18)$$

obeys the equation

$$\psi'' + \frac{1}{\rho}\psi' = -\frac{1}{\lambda_D^2}[\exp(\psi_* - \psi) - 1 - \gamma], \quad (19)$$

with the boundary conditions  $\psi(0)=e\varphi(0)/T \equiv \psi_*$ ,  $\psi'(0)=0$ . The parameter

$$\gamma = -2\omega(\Omega_0 + \omega)/\omega_{p*}^2 - 1 \quad (20)$$

effectively determines the radius of the plasma column for given values of the angular frequency of rotation,  $\omega$ , the cyclotron frequency,  $\Omega_0=eB_0/mc$ , and the plasma frequency,  $\omega_{p*}=\sqrt{4\pi e^2 n_*/m}$ . Localized solutions exist if  $\gamma > 0$ . For a small and positive  $\gamma$  the effective potential near the plasma

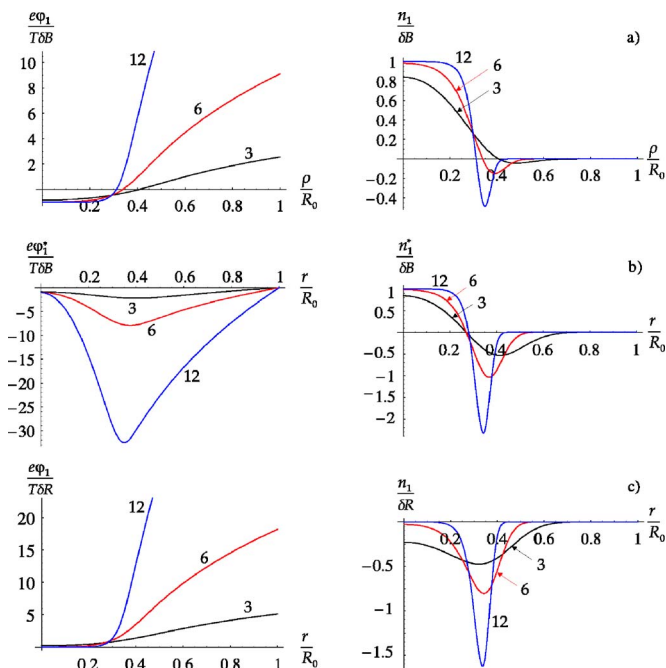


FIG. 4. (Color online) Perturbed potential and density for different ratios of plasma radius to Debye length (indicated directly on the plots). The parameters are the same as in Fig. 2. Magnetically induced perturbations are shown as a function of the flux radius  $\rho$  in (a), and as a function of the cylindrical radius  $r$  in (b), respectively. Electrostatically induced perturbations are shown in (c); in this case  $\rho=r$ . Note that  $\phi_1(R_0) \neq 0$  (a, left) since the flux radius of the wall is equal to  $(1+\delta B/2)R_0$  rather than  $R_0$ ; on the contrary, the perturbed potential  $\phi_1^*(r)$  (b, left) tends to 0 at  $r=R_0$ , as expected. The magnetically induced perturbation of the electric potential tends to  $-(T/e)\delta B$  on the axis if  $a_{1/2}/\lambda_D \geq 3$ , while electrostatically induced perturbations are shielded at the column edge.

column has the form  $\psi(\rho) = \psi_s + \gamma[I_0(\rho/\lambda_D) - 1]$ , and the plasma radius can be roughly evaluated as  $a_0 \sim \lambda_D \ln(1/\gamma)$ . The condition  $\gamma=0$  gives a quadratic equation which determines the frequency of plasma rotation,  $\omega$ , in the fluid limit.<sup>13</sup> The equation has two real solutions,  $\omega = -\Omega_0/2 \pm \sqrt{\Omega_0^2/4 - \omega_{p*}^2/2}$ , provided that the plasma density is below the Brillouin limit,  $\omega_{p*}^2 < \Omega_0^2/2$ . Experiments mainly deal with the low frequency branch, which represents a rigid body rotation with electric drift frequency,  $\omega = -\omega_{p*}^2/2\Omega_0$ , if  $\omega_{p*}^2 \ll \Omega_0^2/2$ .

Numerically computed profiles of  $\phi_0$  and  $n_0$  for a set of parameters relevant to CamV experiment are shown for a fixed plasma radius and different Debye lengths in Fig. 2, and for different plasma radii at fixed Debye length in Fig. 3, respectively. The corresponding profiles for the perturbed electric potential and density, computed from the linearized equations (12a) and (12b), are shown in Fig. 4 and in Fig. 5, respectively.

The perturbation of the electric potential  $\phi_1$  induced by a magnetic field variation with a relative amplitude  $\delta B$ , changes its sign within the plasma boundary for all the values of  $\lambda_D$  considered in Fig. 4 (for a fixed plasma radius,  $a_{1/2}$ , computed at the level of 1/2 of the maximum density) even if condition (17) is not satisfied. However, for fixed  $\lambda_D$  (as in Fig. 5), the sign reversal actually disappears when the plasma radius becomes small in approximate agreement with the condition (17).

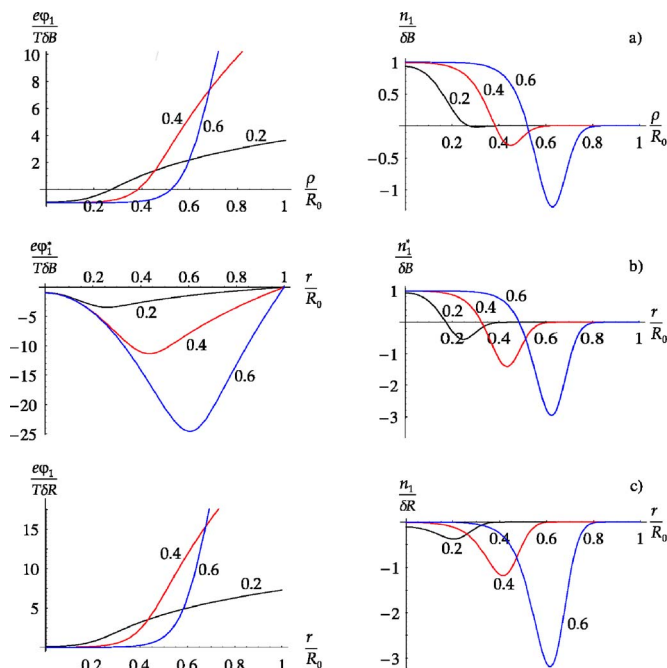


FIG. 5. (Color online) Perturbed potential and density for different ratios of plasma radius to wall radius. The parameters are the same as in Fig. 3.

For magnetically induced perturbations, both  $\phi_1$  and  $\phi_1^*$  tend to  $-\delta B$  at  $r=0$ , if  $\lambda_D \ll a_{1/2}$ . On the contrary, electrostatically induced perturbations, characterized by the relative amplitude  $\delta R$  of the variation of the conducting wall radius, are shielded by the perturbed electric charge at the column edge, so that  $\phi_1 \rightarrow 0$  at  $r=0$  as  $a_{1/2}/\lambda_D \rightarrow \infty$ .

Since the potential and density perturbations induced by a magnetic field variation reverse sign near the plasma edge, in the region of a magnetic squeeze ( $\delta B > 0$ ), the plasma column is "thinner" than what is expected from simply following the magnetic field lines, as it was first noted by Fajans.<sup>10</sup>

A "potential squeeze," characterized by a positive potential variation at the wall,  $\phi_1(R_0) > 0$ , formally corresponds to a positive amplitude  $\delta R$ , since  $\phi_1(R_0)/\delta R = -\phi_0'(R_0)R_0 > 0$ . As shown in Figs. 4(c) and 5(c), a potential squeeze makes the plasma column "thinner" as well, as in the case of a magnetic squeeze. However, near the column's axis the density change is generally smaller and has an opposite sign with respect to the case of a magnetic squeeze.

Since  $\phi_1/\delta B < 0$  in the bulk of the plasma, the global thermal equilibrium state of a non-neutral plasma confined in a magnetic mirror field exhibits another curious feature, qualitatively discussed in Ref. 10. If  $a_{1/2}/\lambda_D \geq 3$ , the plasma density increases linearly with the mirror ratio, so that the plasma is denser in the high magnetic field region since the magnetic squeeze forms a potential trap for low energy particles.

The function  $\phi_1$  nowhere exceeds the value of  $\delta B$  within the plasma column. On the contrary, the amplitude of  $\phi_1^*$  inside the plasma reaches a much greater value near the column edge, where  $\phi_1^* \sim (a_{1/2}/\lambda_D)^2 \delta B$ . As a consequence, within the range of validity of the 1D approximation [characterized by a smooth and small magnetic field perturbation

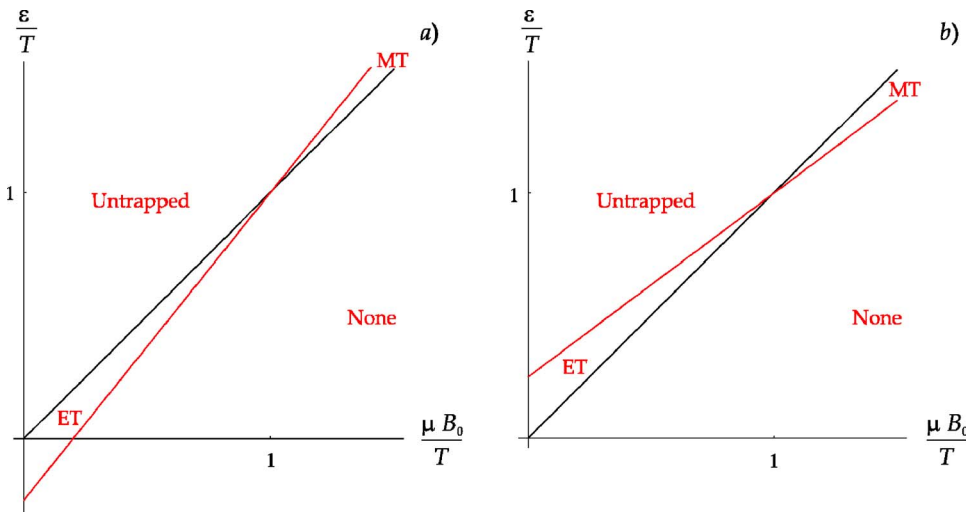


FIG. 6. (Color online) (a) Phase space for the case of a magnetic squeeze,  $\delta B > 0$ . ET, electrostatically trapped particles, located within the magnetic squeeze; MT, magnetically trapped particles, reflected from the magnetic squeeze. (b) Phase space for the case of a magnetic trap,  $\delta B < 0$ . ET, electrostatically trapped particles, reflected from the potential squeeze at the magnetic well; MT, magnetically trapped particles, localized within the magnetic well.

$\delta B(z)$ ], the evaluation of the small quantity  $\phi_1(\rho, z)$  from realistic 2D simulations of the potential  $\phi(r, z)$  requires a very high accuracy of computation. 2D plasma equilibrium simulations will be shown in Sec. V to evaluate the accuracy of the 1D theory.

### C. Anisotropic plasma

Experimentally, a non-neutral plasma may remain anisotropic for a relatively long time, with the longitudinal temperature typically strongly exceeding the perpendicular temperature,  $T_{\parallel} \gg T_{\perp}$ .<sup>14</sup> The opposite case,  $T_{\parallel} \ll T_{\perp}$ , may also have its own peculiarities. The previous discussion can readily be extended to a non-neutral plasma with a bi-Maxwellian distribution function

$$f(\varepsilon, \mu, \rho) = \frac{m^{3/2} N(\rho)}{(2\pi)^{3/2} T_{\parallel}^{1/2} T_{\perp}} \exp\left[-\frac{\varepsilon - \mu B_0}{T_{\parallel}} - \frac{\mu B_0}{T_{\perp}}\right]. \quad (21)$$

In this case

$$n = N(\rho) \exp(-e\varphi/T_{\parallel}) \left[ \frac{T_{\parallel} B}{(T_{\parallel} - T_{\perp}) B_0 + T_{\perp} B} \right]. \quad (22)$$

Poisson's equation (11a) for the unperturbed electric potential remains formally valid for a redefined function  $\phi_0 = e\varphi_0/T_{\parallel}$  and a Debye length  $\lambda_D = \sqrt{T_{\parallel}/4\pi e^2 n_s}$ . Equation (12a) for the perturbed potential  $\phi_1 = e\varphi_1/T_{\parallel}$  is only slightly modified,

$$\frac{1}{\rho} \frac{\partial}{\partial \rho} \rho \frac{\partial \phi_1}{\partial \rho} = \frac{N_0(\rho)}{\lambda_D^2} \left( \phi_1 + \frac{T_{\perp}}{T_{\parallel}} \delta B \right), \quad (12a')$$

while the boundary condition (12b) at the conducting wall remains unchanged. Thus, the magnetic perturbation  $\delta B$  enters the boundary-value problem multiplied by the factor  $T_{\perp}/T_{\parallel}$ , but through the boundary conditions at the wall without this factor. The effect of these boundary conditions is effectively shielded on the plasma edge if  $\lambda_D$  is small in comparison with the plasma radius. One can therefore expect that  $\phi_1 \approx -(T_{\perp}/T_{\parallel}) \delta B$  in the bulk of the plasma. This means that a magnetic perturbation induces a potential perturbation  $\varphi_1 \approx (T_{\perp}/e) \delta B$  near the column axis, which is proportional to  $T_{\perp}$ .

### D. Fraction of trapped particles

As noted in Ref. 10, two distinct groups of trapped particles exist: particles with low parallel energy are trapped in the low magnetic field region (magnetic trap), while particles with low total energy are trapped in the high field region (magnetic squeeze).

In this section the fraction of trapped particles is computed for the Maxwellian distribution (4) with a low temperature ( $a_{1/2} \gg \lambda_D$ ), and when the perturbation of the electric potential  $\phi_1 = -\delta B$  is uniform over the radius  $r$  except for a narrow region close to the plasma column edge with a width of the order of  $\lambda_D$ . Assuming that  $\phi_1 = -\delta B$ , the fraction of particles which are trapped within the perturbed region or reflected from the region, is computed separately for a magnetic squeeze,  $\delta B > 0$ , and a magnetic well,  $\delta B < 0$ .

#### 1. Magnetic squeeze

A magnetic squeeze,  $\delta B = B_1/B_0 > 0$ , creates a potential well for the particles with small magnetic moment since  $\phi_1 = -B_1/B_0 < 0$ . Electrostatically trapped particles are located within the region ET in Fig. 6(a). Particles with a greater magnetic moment are reflected from the magnetic squeeze; they can be thought of as magnetically trapped outside of the magnetic squeeze region. Magnetically trapped particles occupy the region MT; the trapped particles are located between the lines  $\varepsilon = \mu B_0$  and  $\varepsilon = \mu(B_0 + B_1) + \phi_1$ , which intersect in the point  $\varepsilon = \mu B_0 = T$ . Consequently, electrostatically trapped particles have an energy below the plasma temperature,  $\varepsilon < T$ , while magnetically trapped particles are characterized by a higher energy,  $\varepsilon > T$ .

Electrostatically trapped particles are spatially separated from magnetically trapped particles. The former are located within the magnetic squeeze, where the magnetic field is equal to  $B_0 + B_1$  and the electric potential is  $\phi_1 = -B_1/B_0$ . The latter are located outside of the magnetic squeeze, in a region characterized by the unperturbed magnetic field  $B_0$  and  $\phi_1 = 0$ . Hence, the density fraction of electrostatically trapped particles is

$$\begin{aligned} \frac{n_{et}}{n} &= \frac{4\pi(B_0 + B_1)}{\sqrt{2m^{3/2}}} \int_0^{T/B_0} d\mu \int_{-TB_1/B_0 + \mu(B_0 + B_1)}^{\mu B_0} \\ &\times \frac{d\varepsilon \exp(-\varepsilon/T)}{\sqrt{\varepsilon + TB_1/B_0 - \mu(B_0 + B_1)}} \\ &\approx (2/\sqrt{\pi} - \operatorname{erf} i(1)/e) \sqrt{B_1/B_0} = 0.52 \sqrt{B_1/B_0}, \end{aligned} \quad (23)$$

while the fraction of magnetically trapped particles is given by

$$\begin{aligned} \frac{n_{mt}}{n} &= \frac{4\pi B_0}{\sqrt{2m^{3/2}}} \int_{T/B_0}^{\infty} d\mu \int_{\mu B_0}^{-TB_1/B_0 + \mu(B_0 + B_1)} \frac{d\varepsilon \exp(-\varepsilon/T)}{\sqrt{\varepsilon - \mu B_0}} \\ &\approx \sqrt{B_1/B_0} e = 0.37 \sqrt{B_1/B_0}, \end{aligned} \quad (24)$$

where  $\operatorname{erf} i(x)$  is the imaginary error function, and  $e=2.71\dots$  is the base of natural logarithms.

## 2. Magnetic trap

A local depression of the magnetic field,  $\delta B = B_1/B_0 < 0$ , yields a potential squeeze  $\phi_1 = -B_1/B_0 > 0$ . Consequently, the particles with low energies,  $\varepsilon < T$ , marked with the label ET in Fig. 6(b), appear to be electrostatically trapped *outside* of the perturbation region. Hence their fraction has to be calculated for the unperturbed magnetic field  $B_0$  and  $\phi_1 = 0$ :

$$\begin{aligned} \frac{n_{et}}{n} &= \frac{4\pi B_0}{\sqrt{2m^{3/2}}} \int_0^{T/B_0} d\mu \int_{\mu B_0}^{T|B_1|/B_0 + \mu(B_0 - |B_1|)} \frac{d\varepsilon \exp(-\varepsilon/T)}{\sqrt{\varepsilon - \mu B_0}} \\ &\approx (2/\sqrt{\pi} - \operatorname{erf} i(1)/e) \sqrt{|B_1|/B_0} = 0.52 \sqrt{|B_1|/B_0}. \end{aligned} \quad (25)$$

On the contrary, the density of magnetically trapped particles is calculated within the perturbed region, where the magnetic field is  $B - |B_1|$  and the electric potential is given by  $\phi_1 = |B_1|/B_0$ :

$$\begin{aligned} \frac{n_{mt}}{n} &= \frac{4\pi(B_0 - |B_1|)}{\sqrt{2m^{3/2}}} \int_{T/B}^{\infty} d\mu \int_{T|B_1|/B_0 + \mu(B_0 - |B_1|)}^{\mu B_0} \\ &\times \frac{d\varepsilon \exp(-\varepsilon/T)}{\sqrt{\varepsilon - T|B_1|/B_0 - \mu(B_0 - |B_1|)}} \\ &\approx \sqrt{|B_1|/B_0} e = 0.37 \sqrt{|B_1|/B_0}. \end{aligned} \quad (26)$$

Comparing Eq. (23) with Eq. (25), one concludes that the density fraction of electrostatically trapped particles is always equal to  $n_{et}/n = 0.52 \sqrt{|B_1|/B_0}$  independently of whether the trapping is caused by a magnetic squeeze or a well. Similarly, the density fraction of magnetically trapped particles is always  $n_{mt}/n = 0.37 \sqrt{|B_1|/B_0}$ . The ratio  $n_{et}/n_{mt}$  is thus an universal number in contrast to the conclusions of Ref. 10, where it is stated that the fraction of particles trapped in the high field region is typically two to ten times smaller than in the lower field region. The above calculations reveal an opposite situation where the former quantity,  $n_{et}$ , is greater than the latter,  $n_{mt}$ . Note, however, that the fraction of electrostatically trapped particles diminishes as the plasma column radius decreases to few Debye lengths. It is worth noting also that the fraction of all the trapped particles to the total number of particles in the plasma column depends on the length of the perturbation.

For the bi-Maxwellian distribution function (21), the computed fractions of trapped particles must be multiplied by the factor  $\sqrt{T_{\perp}/T_{\parallel}}$ . This makes a natural ‘‘no trapping’’ asymptote for beam-like distribution functions, and may explain the lack of trapped-particle effects in recent experiments.<sup>14</sup>

## IV. DEVIATIONS FROM THE PARAXIAL SOLUTION

Here, the results of the previous section are critically revisited to take into account deviations from paraxiality for a non-neutral plasma in a state of global thermal equilibrium. It is also shown that the previous treatment is valid only in the lowest order in the small ratio  $\omega/\Omega$  and, hence, it must be modified when the rotation frequency  $\omega$  approaches the Brillouin limit.

In thermal equilibrium and for an axisymmetric field, the distribution function depends on the particle energy  $\varepsilon = mv^2/2 + e\varphi(r, z)$  and the canonical momentum  $p_{\theta} = mv_{\theta} r + (em/c)rA_{\theta}(r, z)$ ,

$$f = n_* \left( \frac{m}{2\pi T} \right)^{3/2} \exp \left[ - \frac{\varepsilon - \omega p_{\theta}}{T} \right], \quad (27)$$

where  $n_*$ ,  $T$ , and  $\omega$  are all global constants, which do not explicitly depend on coordinates.<sup>8</sup> Consequently, the plasma density is given by

$$n = n_* \exp(\psi_* - \psi), \quad (28)$$

with the dimensionless potential

$$\psi = \frac{e\varphi}{T} - \frac{m\omega^2 r^2}{2T} - \frac{e\omega r A_{\theta}}{cT} \quad (29)$$

obeying the equation

$$\nabla^2 \psi = - \frac{4\pi e^2 n_*}{T} \exp(\psi_* - \psi) - \frac{2m\omega^2}{T} - \frac{e\omega}{cT} \nabla^2 (rA_{\theta}). \quad (30)$$

It is straightforward to show that

$$\nabla^2 (rA_{\theta}) = 2B_z - \frac{4\pi}{c} r j_{\theta}, \quad (31)$$

where  $j_{\theta} = er\omega n$  is the current density associated with the rigid body rotation of the charged plasma column. Since  $\omega \approx -\omega_p^2/2\Omega_0$ , the ratio between the second and the first term in the RHS of Eq. (31) is exactly equal to  $(\omega r/c)^2 = v^2/c^2$ . Hence, the second term *must* be neglected since it represents a relativistic correction, while a nonrelativistic treatment is considered here, and Eq. (30) finally reduces to

$$\nabla^2 \psi = - \lambda_D^{-2} [\exp(\psi_* - \psi) + 2\omega(\omega + \Omega_z)/\omega_p^{*2}], \quad (32)$$

where  $\omega_p^* = \sqrt{4\pi e^2 n_*/m}$  and  $\Omega_z = eB_z/mc$ . It differs from Eq. (19) for a uniform magnetic field merely by the replacement of the constant  $\Omega_0 = eB_0/mc$  with a given function of the coordinates  $\Omega_z(r, z) = eB_z(r, z)/mc$ . Actually Eq. (32) has been derived by Dubin and O’Neil, though not written explicitly in this final form; cf. Eq. (3.62) in Ref. 3.

### A. Low temperature limit

In a low temperature plasma, where formally  $\lambda_D \rightarrow 0$ , the RHS of Eq. (32) must remain finite. This requirement leads to the equation

$$\exp(\psi_* - \psi) = -2\omega[\omega + \Omega_z(r, z)]/\omega_{p*}^2, \quad (33)$$

which is the same as Eq. (9) in Ref. 15. In contrast to Eq. (32), this equation is valid exclusively in the plasma bulk, where it expresses the density  $n = n_* \exp(\psi_* - \psi)$  as a function of the coordinates  $r$  and  $z$ .

Let the normalization factor  $n_*$  (which enters the definition of  $\omega_{p*}$ ) be chosen so that  $\psi = e\varphi_*/T \equiv \psi_*$  at a reference point  $r=0$ ,  $z=z_*$ , where  $\varphi = \varphi(0, z_*) \equiv \varphi_*$ . The rotation frequency  $\omega$  then obeys the equation

$$1 = -2\omega(\omega + \Omega_*)/\omega_{p*}^2, \quad (34)$$

where  $\Omega_* = \Omega_z(0, z_*)$ . Essentially below the Brillouin limit,  $|\omega| \ll |\Omega_*|/2$ , it has approximate solution

$$\omega \approx -\frac{\omega_{p*}^2}{2\Omega_*} \left[ 1 + \frac{\omega_{p*}^2}{\Omega_*^2} \right]. \quad (35)$$

With the given choice of  $n_*$ , Eq. (33) determines  $\psi$  as function of  $\Omega_z$  and can be used to calculate electric potential and density in the bulk of the plasma. Combining Eq. (29) with (33) and (35), one has

$$e\varphi \approx e\varphi_* - \frac{m\omega_{p*}^2 r A_\theta(r, z)}{2B_*} \left[ 1 + \frac{\omega_{p*}^2}{\Omega_*^2} \right] + \frac{mr^2}{2} \left[ \frac{\omega_{p*}^2}{2\Omega_*} \right]^2 + T \ln \frac{B_*}{B_z(r, z)}, \quad (36)$$

where  $B_* = B_z(0, z_*)$ . The first two terms in Eq. (36) remain constant along a magnetic field line characterized by the flux coordinate  $\alpha = rA_\theta(r, z) = \text{const}$ . Hence, the perturbation of the electric potential along a magnetic field line is described by the remaining two terms, with the last one usually dominating.

For a small perturbation  $B_1 = B_z(\rho, z) - B_*$  of the magnetic field the perturbed part of the electric potential reduces to

$$e\varphi_1(\rho, z) \approx -T[B_1/B_*] \quad (37)$$

in agreement with the results of previous section, with the only difference that  $B_1$  depends now on both  $z$  and  $\rho$ . Being proportional to the plasma temperature  $T$ ,  $e\varphi_1$  does not exceed  $T/e$ . However, for a very low temperature,  $2|\Omega_*|/\omega_{p*} \ll r/\lambda_D$ , the second term in Eq. (36) gives the most significant contribution to the electric potential variation along a magnetic field line:

$$e\varphi_1(\rho, z) \approx -\frac{m\rho^2 \omega_{p*}^4 B_1}{8\Omega_*^2 B_*}. \quad (38)$$

This low temperature regime has never been observed experimentally for a pure electron plasma but might be accessible for a pure ion plasma.

### B. Cold plasma column in a nonuniform magnetic field

Equations (28), (29), and (33) allow us to fully characterize the equilibrium of a cold non-neutral plasma column immersed in a nonuniform magnetic field, which varies slowly along the axial coordinate  $z$ . To describe the equilibrium it is sufficient to note that (1) the plasma density (28) and, hence, the function  $\psi$  are approximately constant across the column,  $r < a$ , and (2) the plasma radius  $a$  varies along  $z$  as the electric potential on the axis,  $\varphi = T\psi/e$ , has to be consistent with the condition (33).

It can readily be shown that the electric potential within a uniform plasma column is equal to

$$\varphi = \frac{m\omega_p^2 a^2}{4e} \left[ 2 \ln \frac{R}{a} + 1 - \frac{r^2}{a^2} \right], \quad (39)$$

where  $a$  and  $R$  are the radius of the column and of the surrounding conducting grounded cylinder, respectively. In the case of a weakly nonuniform magnetic field, Eq. (39) can be used to relate the plasma potential with the local plasma frequency  $\omega_p = \sqrt{4\pi e^2 n/m}$  and the column radius  $a$ . As is deduced from Eqs. (39) and (29), the constancy of the function  $\psi$  across the column section in a given plane  $z$  is provided by the equality

$$\omega_p^2/2 = -\omega(\omega + \Omega_z). \quad (40)$$

Inside the plasma in the same plane, it results in

$$\psi = \frac{m\omega_p^2 a^2}{2T} \ln \frac{R\sqrt{e}}{a}. \quad (41)$$

On the other hand, the plasma density  $n$  in the plane  $z$  is related to the density  $n_*$  in a reference plane  $z=z_*$  by Eq. (28), which can be rewritten for the plasma frequency as

$$\omega_p^2 = \omega_{p*}^2 \exp[-(\psi - \psi_*)]. \quad (42)$$

Being applied to the reference plane, Eq. (40) takes the form  $\omega_{p*}^2/2 = -\omega(\omega + \Omega_*)$ , which determines the rotation frequency  $\omega = (\sqrt{1 - 2\omega_{p*}^2/\Omega_*^2} - 1)\Omega_*/2$ . Equation (40) then yields the plasma density in the arbitrary plane  $z$ .

Equation (41), being applied to the reference plane, expresses  $\psi_*$  by means of the plasma frequency  $\omega_{p*}$  and the column radius  $a_*$  in the same plane. Eliminating  $\psi$ ,  $\psi_*$  and  $\omega_p^2$  from Eq. (42) yields the following equation for the column radius  $a$ :

$$\ln \frac{R\sqrt{e}}{a} - \frac{\omega + \Omega_z}{\omega + \Omega_*} \frac{a^2}{a_*^2} \ln \frac{R\sqrt{e}}{a} = \frac{2T}{m\omega_{p*}^2 a_*^2} \ln \frac{\omega + \Omega_z}{\omega + \Omega_*}. \quad (43)$$

This equation can be further simplified by noting that its RHS is small in the cold plasma limit,  $\lambda_D \ll a$ . The LHS of Eq. (43) contains two factors, both of which result in a smaller plasma radius in the region of a higher magnetic field as compared to the radius expected from the conservation of the magnetic flux,  $\Omega_z a^2 = \Omega_* a_*^2$ . First, this comes as a consequence of the sign of the plasma rotation frequency  $\omega \approx -\omega_{p*}^2/2\Omega_*$ , when using the conservation of the modified flux,  $(\omega + \Omega_z)a^2 = (\omega + \Omega_*)a_*^2$ , introduced in the next section.

Second, the effect of a grounded wall described by the logarithm in the LHS of Eq. (43) leads to an additional decrease of the plasma radius in the high magnetic field region.

### C. Modified Boltzmann law

The treatment of the equilibrium state in Sec. III is based on the assumption that the equilibrium plasma density  $n$  is a function of the magnetic flux  $\alpha$  (or flux radius  $\rho$ ) and the electric potential profile along the field line as in Eq. (5). It is now possible to examine the validity of this assumption for, at least, the case of global thermal equilibrium.

Inserting Eq. (29) into Eq. (28), one obtains

$$n = n_* \exp\left[\frac{m\omega^2 r^2}{2T} + \frac{e\omega r A_\theta}{cT} + \frac{e\varphi_*}{T}\right] \exp\left(-\frac{e\varphi}{T}\right). \quad (44)$$

Since  $\alpha = rA_\theta \approx Br^2/2$ , the above cited assumption is evidently valid if the first term in square brackets can be neglected. This can be done provided that  $\omega \ll \Omega$ , i.e., essentially below the Brillouin limit. The remaining terms in Eq. (44), independent of  $\varphi$ , can then be cast in the desired form as  $N(\alpha) = n_* \exp(e\varphi_*/T + e\omega\alpha/cT)$ .

In the opposite case, one can reuse the computations performed in Sec. III, with a redefined flux coordinate

$$\tilde{\alpha} = rA_\theta + mc\omega r^2/2e \approx (\tilde{B}_* + B_1)r^2/2, \quad (45)$$

where

$$\tilde{B}_* = B_*[1 + \sqrt{1 - 2\omega_p^2/\Omega_*^2}]/2 \approx B_*[1 - \omega_p^2/2\Omega_*^2]. \quad (46)$$

The flux radius is then given by

$$\tilde{\rho} \approx r[1 + B_1/2\tilde{B}_*] \quad (47)$$

instead of Eq. (7a). Since  $\tilde{B}_* < B_*$ , the effect of a magnetic field perturbation becomes more severe as the plasma density approaches the Brillouin limit,  $\omega_p^2 = \Omega_*^2/2$ , where  $\delta\tilde{B} = B_1/\tilde{B}_*$  becomes two times larger as compared to  $\delta B = B_1/B_*$ .

Note that higher order terms in the paraxial expansion, being retained in Eq. (45), do not depend on  $\tilde{B}_*$ , and  $\tilde{\alpha} = (\tilde{B}_* + B_1)r^2/2 - B_1^2 r^4/16 + \dots$ . This means that redefining the flux, as described above, justifies the assumption (5) for arbitrary axisymmetric fields but with  $\alpha$  replaced by  $\tilde{\alpha}$ :

$$n = N(\tilde{\alpha}) \exp(-e\varphi/T). \quad (48)$$

Boltzmann law in its standard form (5) is not exactly applicable for a non-neutral plasma in thermal equilibrium since the corresponding distribution function (27) is not truly isotropic. The validity of the modified Boltzmann law (48) is a specific feature of the state of global thermal equilibrium, which is isotropic in a system of coordinates co-rotating with the plasma column around its axis. Since the rotating system of coordinates is not inertial, the associated centrifugal force modifies Boltzmann law. An arbitrary non-neutral plasma equilibrium is characterized by differential rotation, with the rotation frequency  $\omega$  being a function of the coordinates. For such an equilibrium, neither Eq. (5) nor Eq. (48) turn out to be exact; however Boltzmann law still can be used as a low-

est order approximation in the small parameter  $\omega/\Omega$ . In particular, this justifies the use of Eq. (5) for a stepwise density profile in Sec. III A.

### V. 2D EQUILIBRIUM COMPUTATIONS

The predictions of the 1D analytical theory, treated in Sec. III B, have been compared to the results of 2D numerical equilibrium computations, whose details are given in the Appendix. In general, excellent agreement (of the order of 0.01%) between the radial profiles of both potential and density is found for realistic plasma parameters (relevant to the CamV device<sup>11</sup> at UCSD) and a strictly uniform magnetic field. The comparison is performed for the radial profiles in a reference plane  $z = z_*$ , which in most cases is located in the middle of the trap,  $z = 0$ . End-column effects become significant only for very short traps, when the length  $L$  becomes comparable with the radius of the trap,  $R_0$  (see Fig. 1).

For the case of uniform magnetic field the quantity  $\gamma$ , being the only parameter entering the 1D theory (see Sec. III B), is computed as

$$\gamma_0 = 4u(1 - v) - 1 \quad (49)$$

by means of the input parameters  $u = -\omega\Omega_0/2\omega_p^2$  and  $v = -\omega/\Omega_0$  used in the 2D simulations.

When the perturbation of the magnetic field (simulated by a single circular magnetic coil placed in the midplane of the plasma column) is switched on (while all other input parameters are kept fixed), the parameter  $\gamma$  is modified to

$$\gamma_* = 4u(1 - v + \delta B_*) - 1, \quad (50)$$

where  $\delta B_*$  is the perturbation of the magnetic field in the reference point  $(0, z_*)$ . When this effective value of  $\gamma$  is used in the 1D computations, a very good agreement is obtained again for the radial profiles of density and potential between the 1D and 2D simulations. On the contrary, the use of the “unperturbed” relation (49) results in a non-negligible change of the plasma radius and the electric potential. Indeed, if the plasma radius is large as compared to the Debye length,  $\gamma$  is exponentially small, so that a very small  $\delta B_*$  changes  $\gamma$  by the comparable amount  $\gamma_* - \gamma_0 \approx \delta B_*$  (recall that  $u \approx -1/4$ ). For realistic values of the coil’s radius and the amplitude of the magnetic field perturbation (as used in the CamV experiment), a clear variation of plasma radius is found even if the reference point  $(0, z_*)$  is placed at the end of the plasma column, i.e., at the maximum allowed distance from the perturbation coil. This makes also difficult the comparison of 1D theory with 2D computations, since the former implicitly assumes the existence of a region where the magnetic field can be treated as uniform. Therefore the reference point was finally placed at the geometrical center  $(0, 0)$  of the perturbation coil, i.e., in the midplane of the plasma column; with this choice, the parameter  $\delta B_*$  is equal to the amplitude  $\epsilon$  of magnetic field perturbation, used as an input parameter in the 2D equilibrium code.

Radial and axial profiles of perturbed potential and densities, produced by a magnetic squeeze with an amplitude  $\delta B = \epsilon = 0.1$ , are shown in Figs. 7 and 8, respectively, for parameters relevant to the CamV device. The small difference

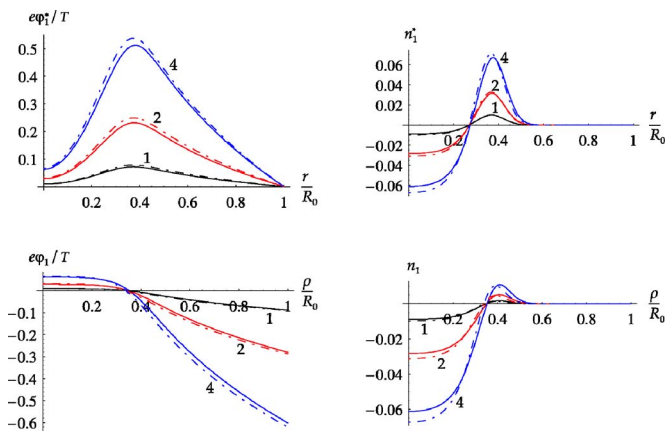


FIG. 7. (Color online) Radial profiles of perturbed electric potential (left) and plasma density (right), 2D simulation (solid curves) vs 1D theory (dashed curves). The black, red, and blue curves refer to  $z/R_0=1, 2$ , and  $4$ , respectively (indicated on the plot).  $N_r=106$  and  $N_z=291$  are used in the 2D simulations. The parameters (relevant to the CamV device) are the following:  $L_{\text{plug}}=5$  cm,  $L=29$  cm,  $R_0=3.5$  cm,  $r_c=13$  cm,  $u=-0.23$ ,  $v=10^{-4}$ ,  $\epsilon=0.1$ ,  $z_*=0$  cm,  $n_* = 1.5 \times 10^7$  cm $^{-3}$ ,  $T=1$  eV; see Fig. 1 for the geometry of the computational region. With these parameters,  $\gamma = -8.009 \times 10^{-2} < 0$ , so that the “unperturbed” 1D equilibrium does not exist. Nevertheless the 1D theory for the effective value  $\gamma_{\text{eff}} = 1.191 \times 10^{-2}$  yields profiles of density and potential (not shown here) very close to those obtained in the 2D simulation.

between the perturbations extracted from the results of the 2D computations and the predictions of the 1D theory (solid and dashed lines, respectively), is within the accuracy of the 1D theory, which is intrinsically linear over the perturbation amplitude  $\epsilon$ . The plasma radius  $a_{1/2}$ , computed at the level of  $1/2$  of the maximum density in the reference plane, coincides within the accuracy of  $0.02\%$  with that predicted by 1D theory for  $\gamma = \gamma_*$ , while the electric potential  $\phi_*$  in the reference point agrees within  $0.1\%$ .

## VI. SUMMARY AND CONCLUSIONS

In summary, a paraxial theory of the equilibrium of a non-neutral plasma for weak axial perturbations of magnetic and electric fields has been developed. Various radial plasma density profiles have been considered, including the case of global thermal equilibrium.

It has been shown that a magnetic barrier (trap) with a relative amplitude  $\delta B = B_1/B_0 > 0$  ( $\delta B < 0$ ) creates a potential trap (barrier) with a depth (height)  $\phi_1 \approx -(T/e)\delta B$  in the plasma bulk, if the plasma radius  $a_{1/2}$  exceeds approximately 3 Debye lengths. On the contrary, the perturbation of the electric potential induced by a variation of the conducting wall radius (or, alternatively, by a variation of the potential distribution over the cylindrical wall of the confining chamber) is effectively shielded inside the plasma column, being localized in a region with a width of the order of few Debye lengths at the plasma edge. In particular, it has been pointed out that a magnetically induced perturbation of the electric potential usually changes its sign at a certain radius within the column edge, while electrostatically induced perturbations never experience this sign reversal (their amplitude monotonically rises towards the confining conducting wall).

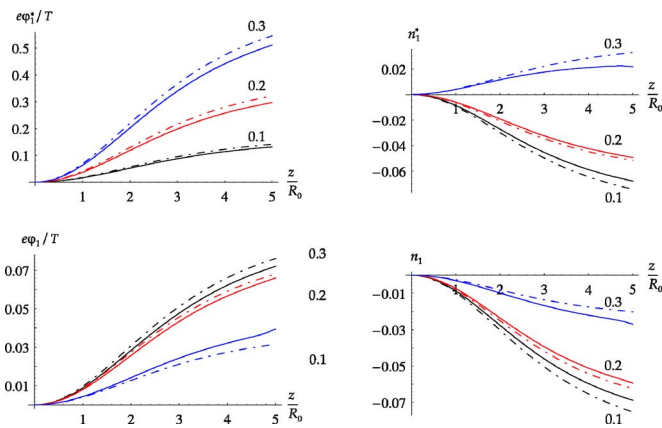


FIG. 8. (Color online) Axial profiles of perturbed electric potential (left) and plasma density (right), 2D simulation (solid curves) vs 1D theory (dashed curves). The black, red, and blue curves refer to  $r/R_0=0.1, 0.2$ , and  $0.3$ , respectively (indicated on the plot). The parameters of the 2D simulation are the same as in Fig. 7.

The analysis has been extended to the case of an anisotropic plasma, finding in particular that the amplitude of a magnetically induced perturbation of the electric potential on a given magnetic field line is proportional to the perpendicular temperature  $T_{\perp}$ , i.e.,  $\phi_1 \approx -(T_{\perp}/e)\delta B$ , while the corresponding variation of the electric potential for a given radius is  $a_{1/2}^2/\lambda_D^2$  times larger, reaching the maximum amplitude at the plasma edge.

The size  $e\phi_1 \approx -T_{\perp}\delta B$  of magnetically induced perturbations of the electrostatic potential along a given magnetic field line is consistent with recent experimental results from the CamV apparatus. In essence, the trapped-particle mediated damping of classical diocotron modes is proportional to the longitudinal particle transport across the trapping separatrix in velocity space. Altering the separatrix at low  $v_{\parallel}$  by a small, externally applied electric squeeze  $V_{\text{sq}}$ , a displaced exponential decrease [see Eq. (7) in Ref. 10] of the damping rate  $\gamma(V_{\text{sq}}) \propto \exp[-ke(V_{\text{sq}} - V_{\text{sq}}^*)/\delta B T_{\perp}]$  has been observed with the offset  $e\phi_1 = keV_{\text{sq}}^* \approx -T_{\perp}\delta B$ , where  $k \ll 1$  is a small factor that describes Debye shielding of the wall potential  $V_{\text{sq}}$  inside the plasma column.

The fractions of magnetically and electrostatically trapped particles created by the external axisymmetric perturbations have been computed explicitly for the case of Maxwellian and bi-Maxwellian distribution functions. Rather surprisingly, the fraction of trapped particles of both kind turns out to be independent from the sign of the magnetic perturbation. Only the total energy of the particles is modified by the presence of the perturbation. More specifically, in the case of a magnetic squeeze magnetically trapped particles have an energy greater than the plasma temperature  $T_{\perp}$ , while the energy of electrostatically trapped particles is smaller than  $T_{\perp}$ . The opposite situation is found in the case of a magnetic trap.

It has been pointed out that a magnetically induced variation of the electric potential in a pure ion plasma might become independent of plasma temperature if  $|\Omega|/\omega_p < a_{1/2}/\lambda_D$ ; in that case  $\phi_1 = -(mr^2\omega_p^4/8e\Omega^2)\delta B$ . This regime

has not yet been observed experimentally and, hence, deserves further investigation.

Several phenomena that lead to deviation from paraxial equilibria have been discussed, including nonparaxial effects per se and the high density case, showing that the amplitude of magnetically induced perturbation doubles as the plasma density approaches the Brillouin limit,  $\omega_p^2 = \Omega^2/2$ .

2D numerical simulations of the thermal equilibrium of a pure electron plasma in the presence of axial magnetic field perturbations have been performed for parameters relevant to the CamV experiment at UCSD, to check the limits of validity of the analytical 1D approximation.

The next goal is to extend the present approach to treat asymmetric perturbations. It is suggested here that the use of flux coordinates will make the interpretation of the results much easier and that it will provide the best approach to the problem of field errors mediated transport of a non-neutral plasma. The results of Sec. III and V evidently support this conclusion.

## ACKNOWLEDGMENTS

The authors are grateful to Dr. Yu. Tsidulko for helpful discussions.

This work was supported by U.S. Civilian Research and Development Foundation Grant No. RUP1-2631-NO-04. A.K. also acknowledges support from the NSF Grant No. PHY0354979.

## APPENDIX: NUMERICAL COMPUTATION OF 2D THERMAL EQUILIBRIA

Numerically, the adimensional equation

$$\phi_{i,j}^{n+1} = (1 - \tau)\phi_{i,j}^n + \frac{\tau}{2(1/\Delta r^2 + 1/\Delta z^2)} \left[ \frac{(1 + \Delta r/2r_i)\phi_{i+1,j}^n + (1 - \Delta r/2r_i)\phi_{i-1,j}^{n+1} + \frac{\phi_{i,j+1}^n + \phi_{i,j-1}^{n+1}}{\Delta z^2} - g(r_i, z_j, \phi_{i,j}^n)}{\Delta r^2} \right],$$

where updated values of  $\phi$  are used as soon as they are available, and  $\tau$  is a relaxation acceleration factor, with  $1 \leq \tau < 2$ .<sup>16</sup>

A fixed electrostatic potential has been imposed on the external boundary of the computation region:  $\phi(r, \pm L) = V_{\text{plug}}$  at the end plates,  $z = \pm L$ , and  $\phi(R_0, z) = 0$  at the conducting external wall, except at the location of the plugs  $|z| > L - L_{\text{plug}}$ , where  $\phi(R_0, z) = V_{\text{plug}}$ .

Azimuthal symmetry around the axis  $r=0$  leads to the boundary condition  $\partial\phi/\partial r=0$  at the ‘‘internal’’ boundary  $r=0$ . An accurate boundary conditions can be derived directly from Poisson’s equation (49):

$$\nabla^2\phi = g(r, z, \phi) \equiv -\exp[-(\phi - \phi_*) - u(1 - v)r^2 - 2ur\delta A_\theta] \quad (A1)$$

is solved to find the 2D thermal equilibrium state, where  $\phi = e\varphi/T$  is the normalized potential, the lengths are normalized over  $\lambda_D$ ,  $u \equiv -\omega\Omega_0/2\omega_p^2$ ,  $v \equiv -\omega/\Omega_0$ ,  $\lambda_D = \sqrt{T/4\pi e^2 n_*}$ , and  $n_*$  and  $\phi_* = \phi(0, z_*)$  represent the density and electric potential in a given position on the axis ( $r=0$ ,  $z=z_*$ ), respectively. The term  $r\delta A_\theta$  represents the perturbed magnetic flux normalized over  $B_0\lambda_D^2$ . The results shown in the paper refer to the case of a circular coil of radius  $r_c$ , so that

$$r\delta A_\theta = \epsilon \frac{r_c}{\pi} \sqrt{(r_c + r)^2 + z^2} [(1 - k^2/2)K - E],$$

where  $K = \int_0^{\pi/2} (1 - k^2 \sin^2 \theta)^{-1/2} d\theta$ ,  $E = \int_0^{\pi/2} (1 - k^2 \sin^2 \theta)^{1/2} d\theta$  are full elliptic integrals, with  $k^2 = 4r_c r / [(r_c + r)^2 + z^2]$ . The magnetic field of the coil, normalized over the value of the uniform magnetic field  $B_0$ , is equal to  $\delta B(z) = \epsilon r_c^3 / (z^2 + r_c^2)^{3/2}$  on the coil’s axis  $r=0$ , and  $\delta A_\theta = r\delta B(z)/2$  near the axis. Hence,  $\epsilon = \delta B(0)$  is the relative amplitude of the magnetic field perturbation in the geometrical center of the coil, with coordinates  $r=z=0$ ; the parameter  $\epsilon$  corresponds to  $B_1/B_0$  in 1D theory, stated in Sec. III.

To numerically solve Eq. (A1) an iteration procedure was implemented, slightly improved as compared to that used earlier in Ref. 12. The equation is discretized, using finite differences. The radial and axial grids are defined as  $r_i = i\Delta r$  ( $i=1, \dots, N_r$ ), with  $\Delta r = R_0/N_r$ , and  $z_j = j\Delta z$  ( $j=-N_z, \dots, N_z$ ), with  $\Delta z = L/N_z$ , respectively,  $R_0$  and  $2L$  being the normalized radius and length of the cylindrical trap (see Fig. 1). Starting with a given approximation  $\phi_{i,j}^0$  for the electric potential  $\phi(r, z)$  at the grid points  $(r_i, z_j)$ , the approximation  $\phi_{i,j}^n$ , obtained at the  $n$ th step, is used in the RHS  $f(r, z, \phi)$  of Eq. (49) to produce the next iteration  $\phi_{i,j}^{n+1}$ . The over-relaxation numerical scheme is written explicitly as<sup>16</sup>

$$\phi_{0,j}^{n+1} = \phi_{1,j}^n - \frac{\Delta r^2}{4} \times \left\{ \exp[\phi_{0,j}^{n+1} - \phi_*^n] - \frac{\phi_{0,j+1}^n - 2\phi_{0,j}^n + \phi_{0,j-1}^n}{\Delta z^2} \right\}.$$

In the numerical solution,  $\phi$  and  $\phi_* = \phi(0, z_*)$  are found iteratively for fixed values of  $u, v, \epsilon, n_*, T$  (plus, of course, plug potential  $V_{\text{plug}}$  and geometry dimensions  $R_0, L, L_{\text{plug}}, r_c, z_*$ ) given as input parameters. The iteration procedure appears to be very robust to the choice of the initial approximation. It converges after some hundreds of iterations for a required accuracy better than  $10^{-7}$ .

To retrieve perturbed quantities such as  $\phi_1(\rho, z)$  and  $n_1(\rho, z)$  that appear in the formulation of the 1D theory, computed mesh values  $\phi_{i,j}$  and  $n_{i,j}$  of potential and density, are interpolated to continuous functions of the cylindrical coordinates  $\phi(r, z)$  and  $n(r, z)$ , respectively. The equation  $\rho^2/2 = r^2/2 + r\delta A_\theta(r, z)$ , determining the flux radius  $\rho(r, z)$  as a function of the coordinates, is inverted to express  $r$  as a function of  $\rho$  and  $z$ ,  $r=r(\rho, z)$ . The exact function  $r(\rho, z)$  is used in the computation of the 2D equilibrium, though the paraxial approximation  $r=\rho/\sqrt{1+\delta B(z)}$  provides good accuracy in most practical cases. Inserting  $r(\rho, z)$  into the first argument of the interpolated functions yield the potential  $\phi(\rho, z)=\phi(r(\rho, z), z)$  and density  $n(\rho, z)=n(r(\rho, z), z)$  in flux coordinates. The perturbed potential is then determined as  $\phi_1(\rho, z)=\phi(\rho, z)-\phi(\rho, z_*)$ ; the perturbed density  $n_1(\rho, z)$  is determined similarly.

<sup>1</sup>J. H. Malmberg and C. F. Driscoll, Phys. Rev. Lett. **44**, 654 (1980).

- <sup>2</sup>D. H. E. Dubin and T. M. O'Neil, Phys. Plasmas **5**, 1305 (1998).  
<sup>3</sup>D. H. E. Dubin and T. M. O'Neil, Rev. Mod. Phys. **71**, 87 (1999).  
<sup>4</sup>D. D. Ryutov and G. V. Stupakov, in *Reviews of Plasma Physics*, edited by B. B. Kadomtsev (Consultants Bureau, New York, 1987), Vol. 13, p. 93.  
<sup>5</sup>R. Keinings, Phys. Fluids **27**, 1427 (1984).  
<sup>6</sup>A. Kabantsev and C. F. Driscoll, Phys. Rev. Lett. **89**, 245001 (2002).  
<sup>7</sup>A. Kabantsev and C. F. Driscoll, Rev. Sci. Instrum. **74**, 1925 (2003).  
<sup>8</sup>T. M. O'Neil and C. F. Driscoll, Phys. Fluids **22**, 266 (1979).  
<sup>9</sup>S. A. Prasad and T. M. O'Neil, Phys. Fluids **22**, 278 (1979).  
<sup>10</sup>J. Fajans, Phys. Plasmas **10**, 1209 (2003).  
<sup>11</sup>A. A. Kabantsev, J. H. Yu, R. B. Lynch, and C. F. Driscoll, Phys. Plasmas **10**, 1628 (2003).  
<sup>12</sup>I. A. Kotelnikov, R. Pozzoli, and M. Romé, Phys. Plasmas **11**, 4396 (2000).  
<sup>13</sup>R. C. Davidson, *An Introduction to the Physics of Non-Neutral Plasmas* (Addison-Wesley, Redwood City, 1990).  
<sup>14</sup>D. L. Eggleston, K. J. McMurtry, A. A. Kabantsev, and C. F. Driscoll, Phys. Plasmas **13**, 032303 (2006).  
<sup>15</sup>L. Turner, Phys. Fluids B **3**, 1355 (1991).  
<sup>16</sup>W. H. Press, S. A. Teukolsky, W. T. Vetterling, and B. P. Flannery, *Numerical Recipes in Fortran 77, The Art of Scientific Computing* (Cambridge University Press, Cambridge, 1997), Vol. 1.